



A machine-learning framework for the simulation of nuclear deflection of Planet-Killer-Asteroids

T.I. Zohdi

Department of Mechanical Engineering, University of California, Berkeley, CA, 94720-1740, USA

Available online 20 July 2022

Abstract

As detection capabilities in astronomy have dramatically improved over the last two decades, concerns over Planet-Killer-Asteroids (PKAs) have become widespread, with nuclear weapons being proposed to destroy or deflect asteroids that are on a short-term projected collision course with Earth. Two main mitigation strategies have been proposed:

- **Case 1:** Break up an incoming asteroid into smaller pieces that will disperse widely, resulting in smaller-scale, less detrimental, Earth-impacts or
- **Case 2:** Deflect an incoming asteroid trajectory to avoid collision altogether.

While the two strategies are not mutually exclusive, deflection is a safer strategy, ideally by harnessing all of the released energy from a nuclear device to move the asteroid as a rigid body. However, this case may not be always possible, since the strength of the energy release may break up the asteroid. In this work, the dynamical response of a PKA to a series of ultra-high energy impulses, such as those generated by nuclear devices, is formulated. A rapid iterative Discrete Element Method (DEM) method is developed to describe the deflection and potential breakup of the PKA as a function of a material bonding strength parameter within the asteroid and the magnitude of the applied impulse. The use of DEM allows for fragmentation of the PKA and the ability to compute the trajectories and distribution of the resulting debris field. Finally, a machine-learning algorithm is then developed and combined with the DEM approach to optimize the pulsation strategy for maximum possible safety and success.

© 2022 Elsevier B.V. All rights reserved.

Keywords: Planet-Killer-Asteroids; Modeling; Simulation; Discrete-elements; Machine-learning

Submission for Special Issue of CMAME in honor of J. T. Oden: In honor J. Tinsley Oden, a titan and transformational figure in the field of Computational Science and Mechanics in the 20th and 21st century-no accolades are high enough-*he deserves megatons!*

1. Introduction

As detection capabilities in astronomy have dramatically improved, concerns over Planet-Killer-Asteroids (PKAs, Fig. 1) have become widespread, with nuclear devices being proposed to destroy or deflect asteroids that are on a short-term projected collision course with Earth. Public awareness of this issue dates at least back to the paper of Luis Alvarez [1] that hypothesized that the mass extinction approximately 65 million years ago was asteroid-impact

E-mail address: zohdi@me.berkeley.edu.

<https://doi.org/10.1016/j.cma.2022.115316>

0045-7825/© 2022 Elsevier B.V. All rights reserved.



Fig. 1. Prototypical asteroids. Photos from the publicly available website: <https://www.publicdomainpictures.net/en/hledej.php?hleda=asteroid>.

induced. An event where Earth is hit with a large asteroid is considered a highly probable reason that life, as we know it, could be extinguished on this planet. The three most important groups of near-Earth asteroids are the Apollos, Amors and Atens. They are often carbon-rich, metallic or silicate based. As of 2022, it was estimated that over 95% of near-Earth asteroids one kilometer or larger in diameter have been discovered.¹

1.1. Space programs

Mitigation strategies to avoid the collision of large asteroids with Earth is a central priority for the continued survival of life on this planet. These concerns have helped spur on the launch of a variety of cameras and computers directly connected to telescopes, with asteroid detection being their objective. Many systems now exist, such as the Asteroid Terrestrial-impact Last Alert System (ATLAS), Lincoln Near-Earth Asteroid Research (LINEAR), Near-Earth Asteroid Tracking (NEAT), etc. The LINEAR system alone has discovered 150,000 asteroids. Nearly 20,000 near-Earth asteroids have been detected, including almost 900 more than one kilometer in diameter. In November 2021, NASA launched the Double Asteroid Redirection Test, which will interest Dimorphos (160 m), approximately 10.5 million kilometers away from Earth. While Dimorphos poses no threat to Earth, it provides a test case for crashing a spacecraft into an asteroid to determine if it can change its trajectory. In general, asteroid impact avoidance encompasses methods by which near Earth Objects, which are on a collision course, are deflected. Provided ample warning is given, even slight deflections can make a large difference. There have been a number of contactless (less aggressive) methods proposed, ranging from placing a large spacecraft in the vicinity of an asteroids to gravitationally alter its trajectory, to ion beams and focussed solar energy to ablate material, to attaching rocket thrusters, etc. For a broad survey, see [1–35]. However, for smaller warning time thresholds, more extreme actions are needed, essentially requiring larger energy input. Specifically, the most concerning scenario is a short-term warning, whereby an extremely large force would be needed to deflect an asteroid, which is the subject of this work.

1.2. Nuclear devices

The US National Science and Technology Council has warned that the world is unprepared for an asteroid impact event, and has developed and released the *National Near-Earth Object Preparedness Strategy Action Plan* to better prepare [27–29]. According to expert testimony in the United States Congress in 2013, NASA would require at least five years of preparation before a mission to intercept an asteroid could be launched [30–32]. Unfortunately, this mission is still not fully operable, but is actively being pursued (such as the DART system). As mentioned, the use of nuclear weapons has been proposed as the only viable tool to provide enough energy to mitigate a large asteroid impact. While a nuclear weapon is a more powerful version of a conventional weapon, it has another component, it is thermo-nuclear, thus potentially leading to melting, fissuring, etc. which go beyond simply a blast.

¹ The term *asteroid* generally refers to large (non-planet) objects of the inner Solar System, including those that are co-orbital with Jupiter. Larger asteroids are often called planetoids. For more general details, see <https://en.wikipedia.org/wiki/Asteroid>.

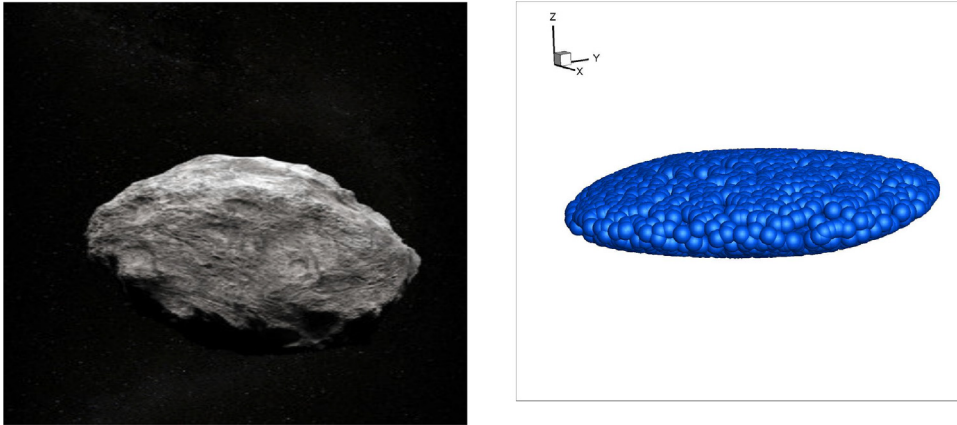


Fig. 2. LEFT: An asteroid (see <https://www.publicdomainpictures.net/en/hledej.php?hleda=asteroid>). RIGHT: A DEM generated PKA via DEM particles. The particles are bound by the mathematical dynamics-constraints to move collectively as a rigid body (group translation and rotation), until a particle is dislodged by an impulse. If it dislodged, it moves according to its own dynamics. The envelope was generated with Eq. (2.1) $(p_1, p_2, p_3) = (4, 4, 1)$ and $(R_1, R_2, R_3) = (0.5, 0.5, 0.1)$.

Approximately 50% is blast energy, 15% nuclear radiation and 35% thermal energy. Thus, approximately 85% of the energy of a nuclear weapon produces air blast (and shock), thermal energy (heat). The remaining 15 percent of the energy is released as various types of nuclear radiation.² The delivered “yield” of such a weapon is typically the amount of energy, calibrated to the relative tons of equivalent TNT (dynamite/ Trinitrotoluene). Commonly used units are kilotons (1000 tons of TNT) and Megatons (1 000 000 tons). A megaton yields 4.18×10^{15} J. The first thermonuclear test yielded approximately 20 kilotons of TNT. Typical bombs yield between 10 and 50 Megatons (the largest ever was the Tsar-Bomba, tested by the USSR in 1961). There are types based on fission and fusion reactions or a combination. For more information, see [33–35]. Regardless of the issues with nuclear devices, they remain the only viable possibility for a *short-term impact mitigation strategy*.

1.3. Mitigation strategies

Two main mitigation strategies have been proposed:

- **Case 1:** Break up an incoming asteroid into smaller pieces that will disperse widely, resulting in smaller-scale, less detrimental, Earth-impacts or
- **Case 2:** Deflect an incoming asteroid trajectory to avoid collision altogether.

While the two strategies are not mutually exclusive, deflection is a safer strategy, ideally by harnessing all of the energy released from a nuclear device to move the asteroid as a rigid body. However, this may not be always possible, since the strength of the released energy may break up the asteroid. *We consider both scenarios.*

1.4. Objectives

In this work, the dynamical response of a PKA to a series of ultra-high energy impulses, such as those generated by nuclear devices, is formulated. A rapid iterative Discrete Element Method (DEM) method is developed to describe the deflection and potential breakup of the PKA as a function of a material bonding strength parameter within the asteroid and the magnitude of the applied impulse. The use of DEM allows for fragmentation of the PKA and the ability to compute the trajectories and distribution of the resulting debris field. Finally, a machine-learning algorithm is then developed and combined with the DEM approach to optimize the pulsation strategy for maximum possible safety and success (see Figs. 2 and 3).

² Thus, one issue is also that the asteroid would be rendered radioactive, which is outside of the present discussion covered in this work.

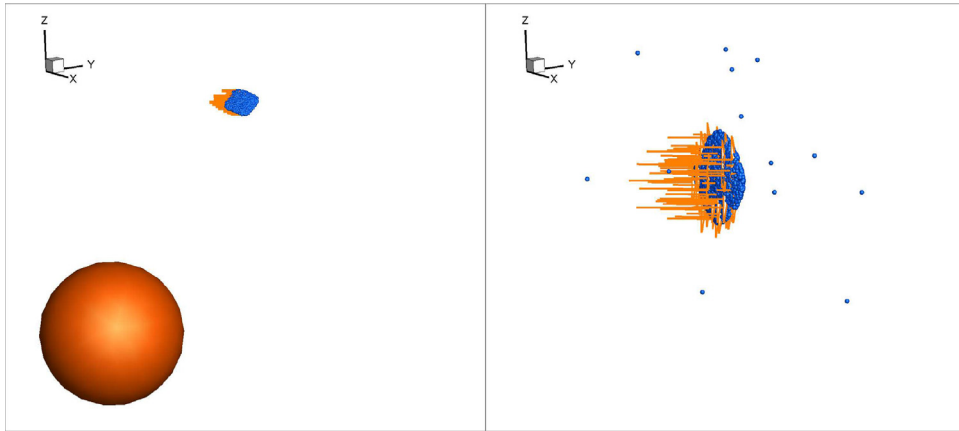


Fig. 3. Left: a frame from the upcoming simulation of the deflection of asteroid headed towards Earth with an impulse applied to the asteroid (orange arrows). Right: a zoom on the impulse-asteroid interaction and resulting fragments. (For interpretation of the references to color in this figure legend, the reader is referred to the web version of this article.)

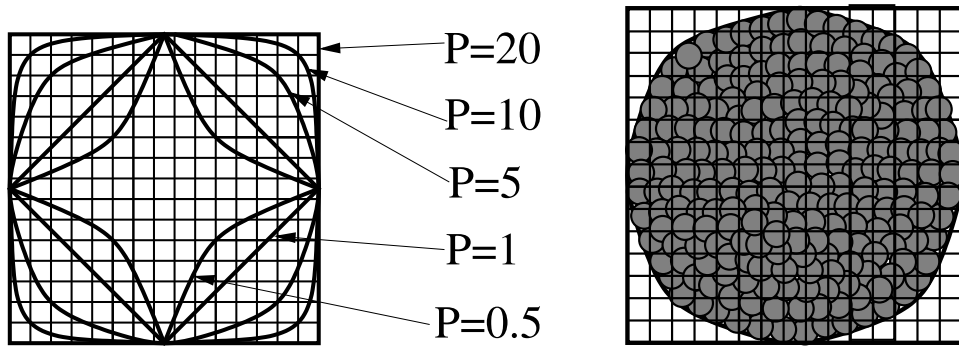


Fig. 4. Generating a PKA hull with discrete elements. This achieved by sweeping through a rectangular parallelepiped of $(\pm R_1, \pm R_2, \pm R_3)$ and checking the intersection of the hull envelope equation above with a box of discrete element position subboxes (left). Where intersections occur, a particle is placed in the subbox (middle). A generalized ellipsoidal equation (Eq. (2.1)) is used where for exponent values of (p_1, p_2, p_3) equal to two, we generate a typical ellipsoid, for values less than one we generate involute (nonconvex shapes), and for exponent values of (p_1, p_2, p_3) greater than two, we generate a box-like shapes (right).

2. Generating an asteroid

To generate the asteroid body, we insert particles within an envelope/grid intersection (Fig. 4). For example, a convenient, easy to parametrize envelope is given by sweeping through a rectangular parallelepiped of $(\pm R_1, \pm R_2, \pm R_3)$ and checking the intersection of the hull envelope equation, for example given by a generalized ellipsoidal equation:

$$\left\| \frac{x_1 - x_{1o}}{R_1} \right\|^{p_1} + \left\| \frac{x_2 - x_{2o}}{R_2} \right\|^{p_2} + \left\| \frac{x_3 - x_{3o}}{R_3} \right\|^{p_3} = 1, \tag{2.1}$$

where (x_1, x_2, x_3) are the coordinates of the DEM particles, (x_1, x_2, x_3) are the coordinates of center of the asteroid, (R_1, R_2, R_3) are the generalized radii and (p_1, p_2, p_3) are exponents of the generalized ellipsoid, with a box of discrete element *subbox* positions (Fig. 4). Where there is an intersection, a particle is placed in the subbox. The particles are initially rigidly bonded together, but may become dislodged due to external forces (discussed later in the presentation). For exponent values of (p_1, p_2, p_3) equal to two, we generate a familiar ellipsoid, for values less than one we generate involute (nonconvex shapes, Fig. 4), and for exponent values of (p_1, p_2, p_3) greater than two, we generate a box-like shapes.

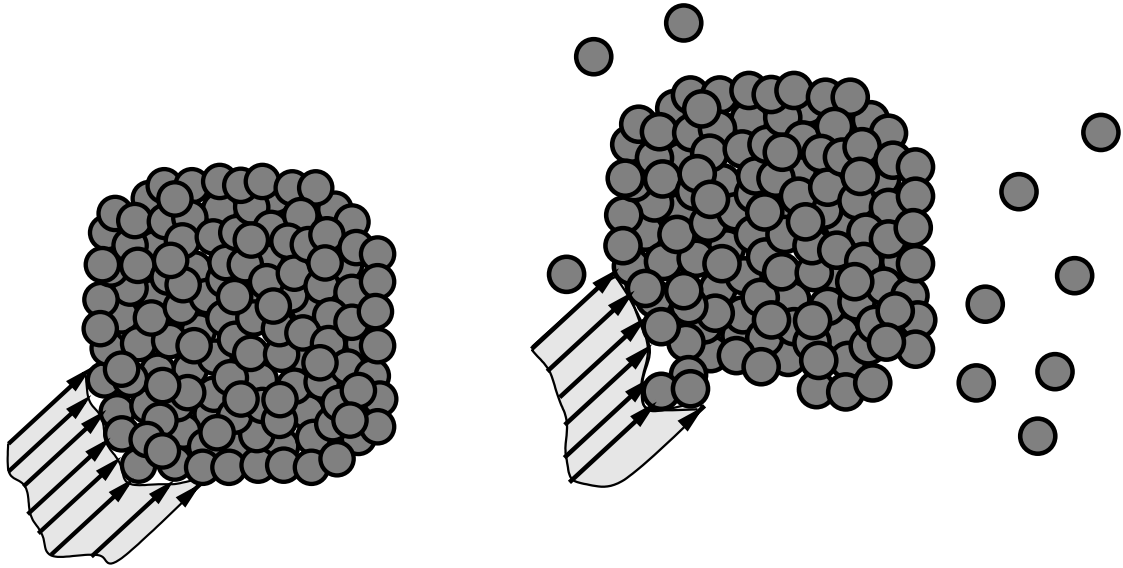


Fig. 5. Left: A system of DEM particles that are rigidly bonded together. Right: Motion and breakup of a cluster from impulses.

3. Dynamics of general rigid clusters of DEM particles

In order to make the analysis general, we consider rigid clusters of DEM particles. Later we will tailor the cluster to specific PKA configurations. We consider the DEM cluster to be already formed, with particles rigidly bonded together. Later, we will allow particles to become dislodged from the cluster. Consider a collection of rigidly-bonded particles, $i = 1, 2, \dots, N_c$, in a cluster. The individual particle dynamics are described by (which leads to a coupled system)

$$m_i \ddot{\mathbf{r}}_i = m_i \dot{\mathbf{v}}_i = \underbrace{\mathbf{F}_i^{tot}}_{\text{total forces}} = \underbrace{\mathbf{F}_i^{int}}_{\text{internal}} + \underbrace{\mathbf{F}_i^{ext}}_{\text{external}}, \quad (3.1)$$

where m_i is the mass of the i th particle, \mathbf{r}_i is the position vector, \mathbf{v}_i is the particle velocity, \mathbf{F}_i^{ext} is an external force field and \mathbf{F}_i^{int} is the sum of the internal (equal in magnitude and opposite in direction) forces acting on the i th particle, due to other particles in the system “internal” particle-to-particle bonding forces, contact forces etc (see Fig. 5).

4. Group dynamics of a rigidly bound collection of particles

When we consider a collection of particles that are bound together as a rigid body, because internal forces between particles within in the system are opposite in direction and equal in magnitude, the specific character of the internal particle-to-particle bonding forces is not relevant to the overall system dynamics, thus

$$\sum_{i=1}^{N_c} (\mathbf{F}_i^{ext} + \mathbf{F}_i^{int}) = \sum_{i=1}^{N_c} \mathbf{F}_i^{ext} + \underbrace{\sum_{i=1}^{N_c} \mathbf{F}_i^{int}}_{=0} = \sum_{i=1}^{N_c} \mathbf{F}_i^{ext} \stackrel{\text{def}}{=} \mathbf{F}^{ext}, \quad (4.1)$$

where \mathbf{F}^{ext} is the overall external force acting on the cluster and N_c are the number of particles in the DEM cluster. The position vector of the center of mass of the system is given by

$$\mathbf{r}_{cm} \stackrel{\text{def}}{=} \frac{\sum_{i=1}^{N_c} m_i \mathbf{r}_i}{\sum_{i=1}^{N_c} m_i} = \frac{1}{M} \sum_{i=1}^{N_c} m_i \mathbf{r}_i, \quad (4.2)$$

where \mathcal{M} is the total system mass. A decomposition of the position vector for particle i , of the form $\mathbf{r}_i = \mathbf{r}_{cm} + \mathbf{r}_{cm \rightarrow i}$, allows the linear momentum of the system of particles (\mathbf{G}) to be written as

$$\sum_{i=1}^{N_c} \underbrace{m_i \dot{\mathbf{r}}_i}_{\mathbf{G}_i} = \sum_{i=1}^{N_c} m_i (\dot{\mathbf{r}}_{cm} + \dot{\mathbf{r}}_{cm \rightarrow i}) = \sum_{i=1}^{N_c} m_i \dot{\mathbf{r}}_{cm} = \dot{\mathbf{r}}_{cm} \sum_{i=1}^{N_c} m_i = \mathcal{M} \dot{\mathbf{r}}_{cm} \stackrel{\text{def}}{=} \mathbf{G}_{cm}, \quad (4.3)$$

since $\sum_{i=1}^{N_c} m_i \dot{\mathbf{r}}_{cm \rightarrow i} = \mathbf{0}$. Furthermore, $\dot{\mathbf{G}}_{cm} = \mathcal{M} \ddot{\mathbf{r}}_{cm}$, thus

$$\dot{\mathbf{G}}_{cm} = \mathcal{M} \ddot{\mathbf{r}}_{cm} = \sum_{i=1}^{N_c} \mathbf{F}_i^{ext} \stackrel{\text{def}}{=} \mathbf{F}^{ext}. \quad (4.4)$$

The angular momentum relative to the center of mass can be written as (utilizing $\dot{\mathbf{r}}_i = \mathbf{v}_i = \mathbf{v}_{cm} + \mathbf{v}_{cm \rightarrow i}$)

$$\sum_{i=1}^{N_c} \mathbf{H}_{cm \rightarrow i} = \sum_{i=1}^{N_c} (\mathbf{r}_{cm \rightarrow i} \times m_i \mathbf{v}_{cm \rightarrow i}) = \sum_{i=1}^{N_c} (\mathbf{r}_{cm \rightarrow i} \times m_i (\mathbf{v}_i - \mathbf{v}_{cm})) \quad (4.5)$$

$$= \sum_{i=1}^{N_c} (m_i \mathbf{r}_{cm \rightarrow i} \times \mathbf{v}_i) - \left(\underbrace{\sum_{i=1}^{N_c} m_i \mathbf{r}_{cm \rightarrow i}}_{=0} \right) \times \mathbf{v}_{cm} = \mathbf{H}_{cm}, \quad (4.6)$$

for a rigid body. Since $\mathbf{v}_{cm \rightarrow i} = \boldsymbol{\omega} \times \mathbf{r}_{cm \rightarrow i}$

$$\mathbf{H}_{cm} = \sum_{i=1}^{N_c} \mathbf{H}_{cm \rightarrow i} = \sum_{i=1}^{N_c} m_i (\mathbf{r}_{cm \rightarrow i} \times \mathbf{v}_{cm \rightarrow i}) = \sum_{i=1}^{N_c} m_i (\mathbf{r}_{cm \rightarrow i} \times (\boldsymbol{\omega} \times \mathbf{r}_{cm \rightarrow i})). \quad (4.7)$$

Decomposing the relative position vector into its components

$$\mathbf{r}_{cm \rightarrow i} = \mathbf{r}_i - \mathbf{r}_{cm} = \hat{x}_{i1} \mathbf{e}_1 + \hat{x}_{i2} \mathbf{e}_2 + \hat{x}_{i3} \mathbf{e}_3, \quad (4.8)$$

where \hat{x}_{i1} , \hat{x}_{i2} and \hat{x}_{i3} are the coordinates of the mass points measured *relative to the center of mass*, and expanding the angular momentum expression, yields

$$\mathbf{H}_1 = \omega_1 \sum_{i=1}^{N_c} (\hat{x}_{i2}^2 + \hat{x}_{i3}^2) m_i - \omega_2 \sum_{i=1}^{N_c} \hat{x}_{i1} \hat{x}_{i2} m_i - \omega_3 \sum_{i=1}^{N_c} \hat{x}_{i1} \hat{x}_{i3} m_i \quad (4.9)$$

and

$$\mathbf{H}_2 = -\omega_1 \sum_{i=1}^{N_c} \hat{x}_{i1} \hat{x}_{i2} m_i + \omega_2 \sum_{i=1}^{N_c} (\hat{x}_{i1}^2 + \hat{x}_{i3}^2) m_i - \omega_3 \sum_{i=1}^{N_c} \hat{x}_{i2} \hat{x}_{i3} m_i \quad (4.10)$$

and

$$\mathbf{H}_3 = -\omega_1 \sum_{i=1}^{N_c} \hat{x}_{i1} \hat{x}_{i3} m_i - \omega_2 \sum_{i=1}^{N_c} \hat{x}_{i2} \hat{x}_{i3} m_i + \omega_3 \sum_{i=1}^{N_c} (\hat{x}_{i1}^2 + \hat{x}_{i2}^2) m_i, \quad (4.11)$$

which can be concisely written as

$$\mathbf{H}_{cm} = \bar{\mathcal{I}} \cdot \boldsymbol{\omega}, \quad (4.12)$$

where we define the moments of inertia with respect to the center of mass

$$\bar{\mathcal{I}}_{11} = \sum_{i=1}^{N_c} (\hat{x}_{i2}^2 + \hat{x}_{i3}^2) m_i, \quad \bar{\mathcal{I}}_{22} = \sum_{i=1}^{N_c} (\hat{x}_{i1}^2 + \hat{x}_{i3}^2) m_i, \quad \bar{\mathcal{I}}_{33} = \sum_{i=1}^{N_c} (\hat{x}_{i1}^2 + \hat{x}_{i2}^2) m_i, \quad (4.13)$$

$$\bar{\mathcal{I}}_{12} = \bar{\mathcal{I}}_{21} = -\sum_{i=1}^{N_c} \hat{x}_{i1} \hat{x}_{i2} m_i, \quad \bar{\mathcal{I}}_{23} = \bar{\mathcal{I}}_{32} = -\sum_{i=1}^{N_c} \hat{x}_{i2} \hat{x}_{i3} m_i, \quad \bar{\mathcal{I}}_{13} = \bar{\mathcal{I}}_{31} = -\sum_{i=1}^{N_c} \hat{x}_{i1} \hat{x}_{i3} m_i, \quad (4.14)$$

or explicitly

$$\bar{\mathcal{I}} = \begin{bmatrix} \bar{\mathcal{I}}_{11} & \bar{\mathcal{I}}_{12} & \bar{\mathcal{I}}_{13} \\ \bar{\mathcal{I}}_{21} & \bar{\mathcal{I}}_{22} & \bar{\mathcal{I}}_{23} \\ \bar{\mathcal{I}}_{31} & \bar{\mathcal{I}}_{32} & \bar{\mathcal{I}}_{33} \end{bmatrix}. \quad (4.15)$$

The particles' own inertia contribution about their respective mass-centers to the overall moment of inertia of the agglomerated body can be described by the Huygens-Steiner (generalized parallel axis theorem) formula ($p, s = 1, 2, 3$)

$$\bar{\mathcal{I}}_{ps} = \sum_{i=1}^{N_c} (\bar{\mathcal{I}}_{ps}^i + m_i (\|\mathbf{r}_i - \mathbf{r}_{cm}\|^2 \delta_{ps} - \hat{x}_{ip} \hat{x}_{is})). \quad (4.16)$$

For a spherical particle, $\bar{\mathcal{I}}_{pp}^i = \frac{2}{5} m_i R_i^2$, and for $p \neq s$, $\bar{\mathcal{I}}_{ps}^i = 0$ (no products of inertia), R_i being the particle radius.³ Finally, for the derivative of the angular momentum, utilizing $\dot{\mathbf{r}}_i = \mathbf{a}_i = \mathbf{a}_{cm} + \mathbf{a}_{cm \rightarrow i}$, we obtain

$$\dot{\mathbf{H}}_{cm}^{rel} = \sum_{i=1}^{N_c} (\mathbf{r}_{cm \rightarrow i} \times m_i \mathbf{a}_{cm \rightarrow i}) = \sum_{i=1}^{N_c} (\mathbf{r}_{cm \rightarrow i} \times m_i (\mathbf{a}_i - \mathbf{a}_{cm})) \quad (4.17)$$

$$= \sum_{i=1}^{N_c} (m_i \mathbf{r}_{cm \rightarrow i} \times \mathbf{a}_i) - \underbrace{\left(\sum_{i=1}^{N_c} m_i \mathbf{r}_{cm \rightarrow i} \right) \times \mathbf{a}_{cm}}_{=0} = \dot{\mathbf{H}}_{cm}, \quad (4.18)$$

and consequently

$$\dot{\mathbf{H}}_{cm} = \frac{d(\bar{\mathcal{I}} \cdot \boldsymbol{\omega})}{dt} = \sum_{i=1}^{N_c} \mathbf{r}_{cm \rightarrow i} \times \mathbf{F}_i^{ext} \stackrel{\text{def}}{=} \mathbf{M}_{cm}^{ext}, \quad (4.19)$$

where \mathbf{M}_{cm}^{ext} is the total external moment about the center of mass.

5. Numerical methods for the dynamics of a DEM cluster

We now treat the dynamics of a cluster numerically. We first focus on the translational motion of the center of mass, and then turn to the rotational contribution.

5.1. DEM cluster translational contribution

The translational component of the center of mass can be written as

$$\mathcal{M} \ddot{\mathbf{r}}_{cm} = \mathcal{M} \dot{\mathbf{v}}_{cm} = \mathbf{F}^{ext}. \quad (5.1)$$

A trapezoidal time-stepping rule is used, whereby at some intermediate moment in time $t \leq t + \phi \Delta t \leq t + \Delta t$ ($0 \leq \phi \leq 1$)

$$\dot{\mathbf{v}}_{cm}(t + \phi \Delta t) \approx \frac{\mathbf{v}_{cm}(t + \Delta t) - \mathbf{v}_{cm}(t)}{\Delta t} \quad (5.2)$$

$$= \frac{1}{\mathcal{M}(t + \phi \Delta t)} \mathbf{F}^{ext}(t + \phi \Delta t) \quad (5.3)$$

$$\approx \frac{1}{\mathcal{M}(t + \phi \Delta t)} (\phi \mathbf{F}^{ext}(t + \Delta t) + (1 - \phi) \mathbf{F}^{ext}(t)), \quad (5.4)$$

where $\mathcal{M}(t + \phi \Delta t) \approx \phi \mathcal{M}(t + \Delta t) + (1 - \phi) \mathcal{M}(t)$, leading to

$$\mathbf{v}_{cm}(t + \Delta t) = \mathbf{v}_{cm}(t) + \frac{\Delta t}{\mathcal{M}(t + \phi \Delta t)} (\phi \mathbf{F}^{ext}(t + \Delta t) + (1 - \phi) \mathbf{F}^{ext}(t)). \quad (5.5)$$

³ If the particles are sufficiently small, each particle's own moment inertia (about its own center) is insignificant, leading to $\bar{\mathcal{I}}_{ps} = \sum_{i=1}^{N_c} m_i (\|\mathbf{r}_i - \mathbf{r}_{cm}\|^2 \delta_{ps} - \hat{x}_{ip} \hat{x}_{is})$.

For the position, we have

$$\dot{\mathbf{r}}_{cm}(t + \phi \Delta t) \approx \frac{\mathbf{r}_{cm}(t + \Delta t) - \mathbf{r}_{cm}(t)}{\Delta t} \approx \mathbf{v}_{cm}(t + \phi \Delta t) \approx (\phi \mathbf{v}_{cm}(t + \Delta t) + (1 - \phi) \mathbf{v}_{cm}(t)), \quad (5.6)$$

leading to

$$\mathbf{r}_{cm}(t + \Delta t) = \mathbf{r}_{cm}(t) + \Delta t (\phi \mathbf{v}_{cm}(t + \Delta t) + (1 - \phi) \mathbf{v}_{cm}(t)). \quad (5.7)$$

5.2. Rotational dynamics

The asteroid’s angular velocity and rotation are determined in a similar manner by integrating the equations for an angular momentum balance

$$\dot{\mathbf{H}}_{cm} = \frac{d(\bar{\mathcal{I}} \cdot \boldsymbol{\omega})}{dt} = \mathbf{M}_{cm}^{ext}, \quad (5.8)$$

where $\bar{\mathcal{I}}$ is the mass moment of the asteroid, $\boldsymbol{\omega}$ is the angular velocity and \mathbf{M}_{cm}^{ext} is the sum of all moment contributions external to the asteroid, around its center of mass. We remark that there are essentially two possible approaches to compute the rotational dynamics; either (1) an inertially-fixed frame or (2) a body-fixed frame. For the discrete element approach, it is advantageous to use an inertially-fixed frame.⁴ The procedure is, within a time step, to decompose an increment of motion into a rigid body translation and rotation about the center of mass. The rotation is determined by solving for the angular velocity and the subsequent incremental rotation of the body around the axis of rotation, which is aligned with the angular velocity vector direction. This leads to a coupled set of nonlinear equations which are solved iteratively. Using a fixed frame of reference for Eq. (5.8) results in $\bar{\mathcal{I}}$ being implicitly dependent on $\boldsymbol{\omega}(t)$, leading to a coupled system of nonlinear ODE’s. These will be solved iteratively. Eq. (5.8) is discretized by a trapezoidal scheme

$$\frac{d(\bar{\mathcal{I}} \cdot \boldsymbol{\omega})}{dt} \Big|_{t+\phi \Delta t} = \frac{(\bar{\mathcal{I}} \cdot \boldsymbol{\omega})|_{t+\Delta t} - (\bar{\mathcal{I}} \cdot \boldsymbol{\omega})|_t}{\Delta t}. \quad (5.9)$$

thus leading to

$$(\bar{\mathcal{I}} \cdot \boldsymbol{\omega})|_{t+\Delta t} = (\bar{\mathcal{I}} \cdot \boldsymbol{\omega})|_t + \Delta t \mathbf{M}_{cm}^{ext}(t + \phi \Delta t). \quad (5.10)$$

Solving for $\boldsymbol{\omega}(t + \Delta t)$ yields

$$\boldsymbol{\omega}(t + \Delta t) = (\bar{\mathcal{I}}(t + \Delta t))^{-1} \cdot ((\bar{\mathcal{I}} \cdot \boldsymbol{\omega})|_t + \Delta t \mathbf{M}_{cm}^{ext}(t + \phi \Delta t)), \quad (5.11)$$

where

$$\mathbf{M}_{cm}^{ext}(t + \phi \Delta t) \approx \phi \mathbf{M}_{cm}^{ext}(t + \Delta t) + (1 - \phi) \mathbf{M}_{cm}^{ext}(t) \quad (5.12)$$

which yields an implicit nonlinear equation, of the form $\boldsymbol{\omega}(t + \Delta t) = \mathcal{F}(\boldsymbol{\omega}(t + \Delta t))$, since $\bar{\mathcal{I}}(t + \Delta t)$, due to the body’s rotation. An iterative, implicit, solution scheme may be written as follows for $K = 1, 2, \dots$

$$\boldsymbol{\omega}^{K+1}(t + \Delta t) = \left(\bar{\mathcal{I}}^K(t + \Delta t)\right)^{-1} \cdot ((\bar{\mathcal{I}} \cdot \boldsymbol{\omega})|_t + \Delta t \mathbf{M}_{cm}^{ext,K}(t + \phi \Delta t)), \quad (5.13)$$

where $\bar{\mathcal{I}}^K(t + \Delta t)$ can be re-computed from the previous formulas.⁵ After the update for $\boldsymbol{\omega}^{K+1}(t + \Delta t)$ has been computed (utilizing the $\bar{\mathcal{I}}^K(t + \Delta t)$ from the previous iteration), the rotation of the body about the center of mass can be determined.

5.3. Iterative superposition scheme-including loss of dislodged particles

The total velocity of any particle can be decomposed into the velocity of the center of mass of the entire object and the rotation of the particle relative to the center of mass:

$$\mathbf{v}_i = \mathbf{v}_{cm} + (\mathbf{v}_i - \mathbf{v}_{cm}) = \mathbf{v}_{cm} + \mathbf{v}_{cm \rightarrow i} = \mathbf{v}_{cm} + \boldsymbol{\omega} \times (\mathbf{r}_{cm} - \mathbf{r}_i) = \mathbf{v}_{cm} + \boldsymbol{\omega} \times \mathbf{r}_{cm \rightarrow i} \quad (5.14)$$

⁴ For a body-fixed formulation, see Powell and Zohdi [36].

⁵ One may view the overall process as a fixed-point calculation of the form $\boldsymbol{\omega}^{K+1}(t + \Delta t) = \mathcal{F}(\boldsymbol{\omega}^K(t + \Delta t))$.

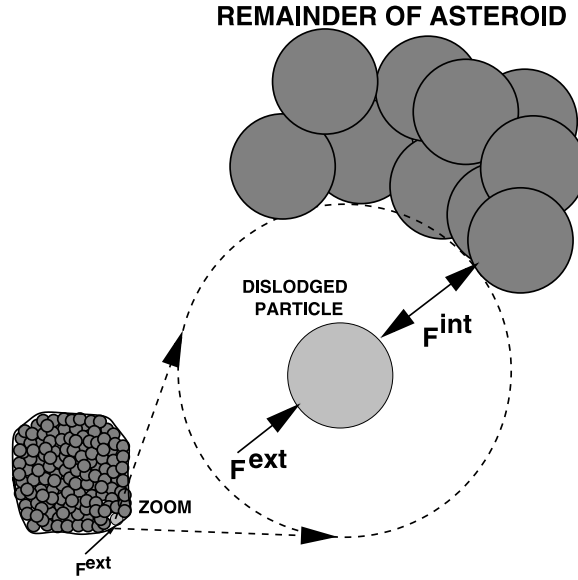


Fig. 6. A freebody diagram of a dislodged particle. As an approximation, we assume that the internal reaction force is collinear with the applied external force.

Explicitly, the overall motion for the bonded particles is computed by $\mathbf{r}_i = \mathbf{r}_{cm} + \boldsymbol{\omega} \times (\mathbf{r}_i - \mathbf{r}_{cm})$, sequentially by computing:

- $\mathbf{C}_1 = \phi \mathbf{v}_{cm}(t + \Delta t) + (1 - \phi) \mathbf{v}_{cm}(t)$,
- $\mathbf{C}_2 = \phi \boldsymbol{\omega}(t + \Delta t) + (1 - \phi) \boldsymbol{\omega}(t)$,
- $\mathbf{C}_3 = \phi \mathbf{r}_{cm}(t + \Delta t) + (1 - \phi) \mathbf{r}_{cm}(t)$,
- $\mathbf{C}_4 = \phi \mathbf{r}_i(t + \Delta t) + (1 - \phi) \mathbf{r}_i(t) - \mathbf{C}_3$,
- $\mathbf{C}_5 = \mathbf{C}_2 \times \mathbf{C}_4$,
- $\mathbf{r}_i(t + \Delta t) = \mathbf{r}_i + \Delta t(\mathbf{C}_1 + \mathbf{C}_5)$,

For particles that have broken off, one calculates

- $\mathbf{v}_i(t + \Delta t) = \mathbf{v}_i(t) + \frac{\Delta t}{m_i} (\mathbf{p}_i(t + \delta t) - m_i \mathbf{g})$,
- $\mathbf{r}_i(t + \Delta t) = \mathbf{r}_i(t) + \Delta t(\phi \mathbf{v}_i(t + \Delta t) + (1 - \phi) \mathbf{v}_i(t))$,

where \mathbf{p}_i is the impulse on the loose particle that was bonded to the rigid body. We assume that a portion of the impulse that hits the rigid body is absorbed by the body, and if the particle is dislodged a portion acts on the loose particle.

5.4. Criteria for asteroid breakup

The criteria used for particle dislodge is a purely local model that avoids a full multibody calculation. It proceeds by:

- Checking the magnitude of an impulse force that the particle experiences.
- If the magnitude exceeds a threshold, the particle is deemed *dislodged* and moves according to its own dynamics.
- The primary issue becomes, what is the load share between the particle and the macroscopic body (Fig. 6), which we approximate.

Accordingly, we approximate the internal reaction force, \mathbf{F}_i^{int} as being collinear with the applied external force, \mathbf{F}_i^{ext} , specifically:

$$\mathbf{F}_i^{int} = -\zeta_i \mathbf{F}_i^{ext} \quad 0 \leq \zeta_i \leq 1, \quad (5.15)$$

where if a threshold dislodging criteria is met, $\|\mathbf{F}_i^{ext}\| \geq F^*$, then $\zeta_i = \frac{F^*}{\|\mathbf{F}_i^{ext}\|}$. Consequently, a force balance on the remainder of the asteroid indicates (including here external forces not associated with the impulse)

$$(M - m_i)\dot{\mathbf{v}}_{cm} = -\mathbf{F}_i^{int} = \zeta_i \mathbf{F}_i^{ext}, \quad (5.16)$$

and on the dislodged particle

$$m_i \dot{\mathbf{v}}_i = \mathbf{F}_i^{ext} - \mathbf{F}_i^{int} = (1 - \zeta_i) \mathbf{F}_i^{ext}. \quad (5.17)$$

5.5. Algorithmic procedure

The overall procedure is as follows, at time t :

1. Generate the asteroid body by inserting particles within the envelope/grid interaction (Fig. 4):

$$\left\| \frac{x_1 - x_{1o}}{R_1} \right\|^{p_1} + \left\| \frac{x_2 - x_{2o}}{R_2} \right\|^{p_2} + \left\| \frac{x_3 - x_{3o}}{R_3} \right\|^{p_3} = 1. \quad (5.18)$$

2. Set initial conditions, if $t = 0$.
3. Compute the new position of the center of mass.
4. Compute (iteratively) the positions of the particles in the body $\mathbf{r}_i^K(t + \Delta t)$, $K = 1, 2, \dots$:

$$\|\mathbf{r}_i^{K+1}(t + \Delta t) - \mathbf{r}_i^K(t + \Delta t)\| \leq TOL \|\mathbf{r}_i^{K+1}(t + \Delta t)\|. \quad (5.19)$$

This requires computation of the position of the center of mass, the rotation of the body, and the calculation of the positions of the particles within the iterations:

- (a) Compute/update: $\mathbf{v}_{cm}^{K+1}(t + \Delta t) = \mathbf{v}_{cm}(t) + \frac{\Delta t}{\mathcal{M}(t + \phi \Delta t)} (\phi \mathbf{F}^{K+1, ext}(t + \Delta t) + (1 - \phi) \mathbf{F}^{ext}(t))$.
 - (b) Compute/update: $\mathbf{r}_{cm}^{K+1}(t + \Delta t) = \mathbf{r}_{cm}(t) + \Delta t (\phi \mathbf{v}_{cm}(t + \Delta t) + (1 - \phi) \mathbf{v}_{cm}(t))$.
 - (c) Compute/update: $\mathbf{M}_{cm}^{ext}(t + \phi \Delta t) \approx \phi \mathbf{M}_{cm}^{ext}(t + \Delta t) + (1 - \phi) \mathbf{M}_{cm}^{ext}(t)$,
 - (d) Compute/update: $\boldsymbol{\omega}^{K+1}(t + \Delta t) = \left(\bar{\mathcal{I}}^K(t + \Delta t) \right)^{-1} \cdot \left((\bar{\mathcal{I}} \cdot \boldsymbol{\omega})|_t + \Delta t \mathbf{M}_{cm}^{ext, K}(t + \phi \Delta t) \right)$,
 - (e) Compute/update: $\mathbf{v}_i = \mathbf{v}_{cm} + \boldsymbol{\omega} \times \mathbf{r}_{cm \rightarrow i}$
 - (f) Compute/update: $\mathbf{r}_i(t + \Delta t) = \mathbf{r}_i + \Delta t (\mathbf{C}_1 + \mathbf{C}_5)$,
 - (g) Repeat steps (a)–(f) until Eq. (5.19) is satisfied.
5. After convergence within a time step, for particles that have broken off, calculate
 - (a) $\mathbf{v}_i(t + \Delta t) = \mathbf{v}_i(t) + \frac{\Delta t}{m_i} (\mathbf{p}_i(t + \delta t) - m_i \mathbf{g})$,
 - (b) $\mathbf{r}_i(t + \Delta t) = \mathbf{r}_i(t) + \Delta t (\phi \mathbf{v}_i(t + \Delta t) + (1 - \phi) \mathbf{v}_i(t))$.
 6. Increment time forward and repeat the procedure.

Remark. A complete, coupled fragmentation analysis, accounting for the stress waves and coupling between the dislodged materials and the remainder of the asteroid is beyond the scope of this paper. For such analyses, we refer the reader to Zohdi [37–42] for details. In such cases, the entire coupled system is solved recursively within each time step, thus producing a fixed point iteration of the form: $\mathbf{r}_i^{K+1}(t + \Delta t) = \mathcal{F}(\mathbf{r}_i^K(t + \Delta t)) + \mathbf{R}$. The convergence of such a scheme scales with the time-step size. For sufficiently small sizes, the scheme converges quite quickly and is second-order accurate. For more details, which necessitate adaptive time-stepping schemes, see [Appendices A and B](#).

6. Parametric numerical examples

We consider a PKA on a direct collision course with Earth, directed from the asteroid's initial center of mass to the Earth's center, in the $\mathbf{n} = (0, 0, -1)$ direction. Due to the disparate magnitude of the numbers in the system,

we normalized the system by the ratio of the actual sized of Earth⁶:

$$\lambda^4 \mathcal{M}^{sim} \dot{\mathbf{v}}_{cm}^{sim} = \lambda^4 \mathbf{F}^{grav,sim} + \mathbf{F}^{pulse,sim}, \quad (6.1)$$

where $\lambda = \frac{R^{actual}}{R^{sim}}$, where $R^{act} = 6,3781,000m$ and $R^{sim} = 1$,

$$\mathcal{M} \dot{\mathbf{v}}_{cm} = \lambda^3 \mathcal{M}^{sim} \lambda \dot{\mathbf{v}}_{cm}^{sim}, \quad (6.2)$$

and

$$\mathbf{F}^{grav} = G \frac{\lambda^3 \mathcal{M}^{sim} \lambda^3 M^{sim}}{\lambda^2 \|\mathbf{r}_{cm}^{sim} - \mathbf{r}^{sim,earth}\|^2} = \lambda^4 \mathbf{F}^{grav,sim}. \quad (6.3)$$

Thus, the impulse parameters should be interpreted as being normalized by $\frac{1}{\lambda^4}$. The following simulation parameters were chosen (length-scales normalized with respect to Earth's radius):

- DEM particles: 5000,
- Total time duration: $T = 10$ s,
- Time step size: $\Delta t = 0.00005$ s,
- Starting position of center of mass: $\mathbf{r}_{cm}(t = 0) = (0, 0, 10)$ m,
- Starting velocity of center of mass: $\mathbf{v}_{cm}(t = 0) = 2$ m/s, directly towards "Earth", centered at $(0, 0, 0)$ m,
- Starting angular velocity: $\boldsymbol{\omega}_{cm}(t = 0) = (1, 1, 1)$ rad/s,
- Time stepping parameter: $\phi = 0.5$ (midpoint rule),
- PKA shape exponents $(p_1, p_2, p_3) = (4, 4, 1)$,
- Size of PKA: $(R_1, R_2, R_3) = (0.1, 0.1, 0.01)$ m,
- Density of the asteroid material: $\rho = 5000$ kg/m³,
- Impulse forces throughout the body: 100 impulses each at $(100, 0, 0) \times (1 + a \times \delta)$, $a=1.0$, $-1 \leq \delta \leq 1$,
- Magnitude of blasts=200,
- Number of blasts: 5 (one every 2 normalized-seconds),
- Fragmentation threshold for dislodging of a particle: 1000 N, 500 N, 200 N, 100 N, 75 N, 50 N etc.

Figs. 7 and 8 illustrate typical results. Table 2 provides quantitative results.⁷ Table 1 illustrates the effects of the β (the bond strength) on (at the end of the simulation time):

- the final asteroid center of mass position: $(r_x^{cm}, r_y^{cm}, r_z^{cm})$,
- the ratio of final asteroid mass to original mass: $\frac{M_f}{M_o}$,
- the number of mass units impacting Earth (intersecting the Earth's surface envelope) and
- the ratio asteroid mass impacting Earth to original asteroid mass (intersecting the Earth's surface envelope): $\frac{M_I}{M_o}$.

In this model problem, the critical bond (scaled) parameter value that transitions the simulation result from pure deflection to deflection and breakup is below between 75–100 N. Clearly, the debris field becomes progressively more dangerous as the bond parameter decreases. Thus, while two main mitigation strategies are plausible: (1) break up an incoming asteroid into smaller pieces that will disperse widely, resulting in smaller-scale, less detrimental, Earth-impacts or (2) deflect an incoming asteroid trajectory to avoid collision altogether, pure deflection, if possible, is a safer strategy, ideally by harnessing all of the released energy from a nuclear device to move the asteroid as a rigid body. Of course, this may not be always possible, since the magnitude of the energy release may break up the asteroid. However, the rapid iterative Discrete Element Method (DEM) method developed here can be combined with a machine-learning method to optimize the pulsation strategy for the maximum possible safety and success.

7. Genetic-based machine-learning for optimal asteroid-mitigation

The rapid rate at which these simulations can be completed enables the ability to explore inverse problems seeking to determine what parameter combinations can deliver a desired result (Fig. 9). In order to ascertain

⁶ The Universal Gravitational constant is 6.6743×10^{-11} , between two bodies (a and b, for example), where $\boldsymbol{\Psi}^{grav} = \frac{GM_a M_b}{\|\mathbf{r}_a - \mathbf{r}_b\|^2}$.

⁷ A standard Macbook Pro laptop was used for all calculations using a code written by the author.

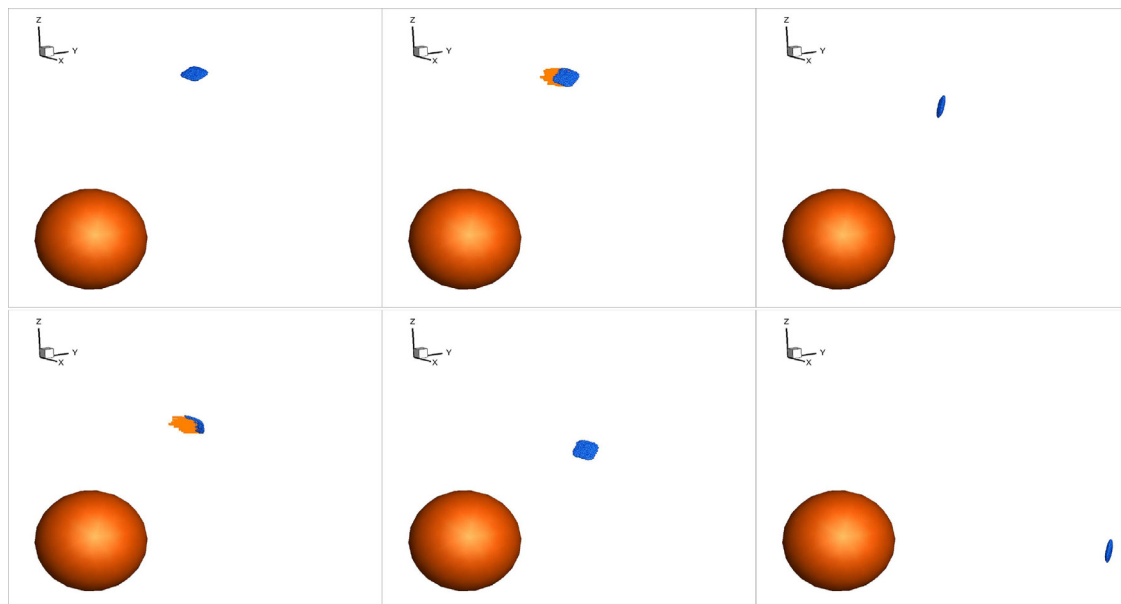


Fig. 7. Starting top left to bottom right: sequence of frames enduring multiple pulses with breakup suppressed.

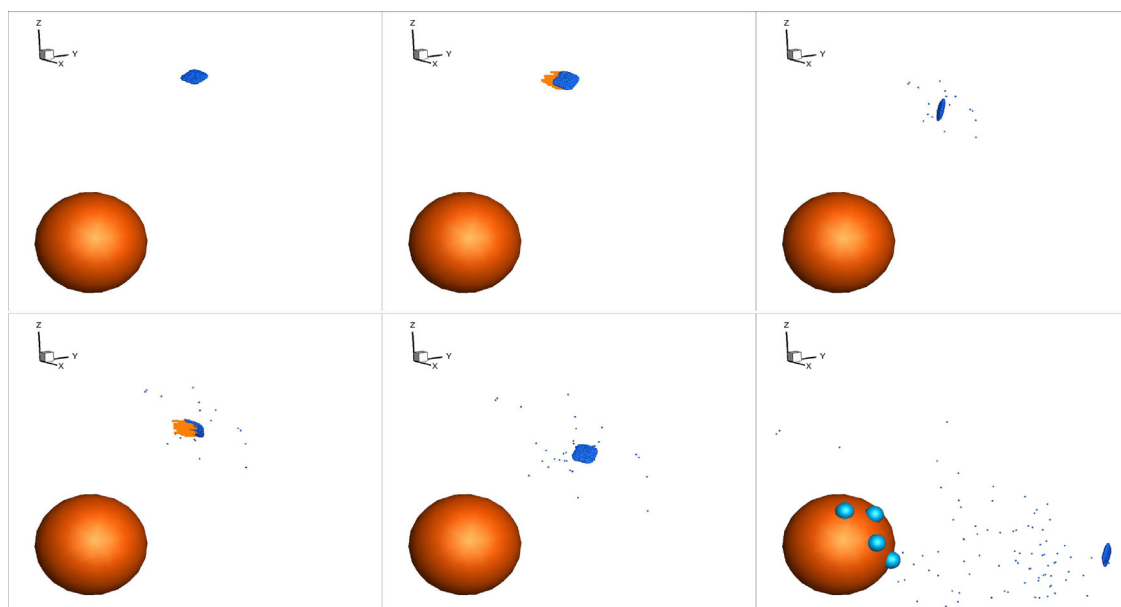


Fig. 8. Starting top left to bottom right: sequence of frames enduring multiple pulses with breakup allowed.

these parameters settings, we develop a genetic-based machine-learning algorithm (MLA), which is well-suited for nonconvex optimization. Following Zohdi [43–47], we formulate the objective as a cost function minimization problem that seeks system parameters that deliver a desired response

$$\Pi(\Lambda_1, \dots, \Lambda_N) \stackrel{\text{def}}{=} w_1 \Pi^{(1)} + w_2 \Pi^{(2)} \stackrel{\text{def}}{=} \Pi^{total}, \tag{7.1}$$

Table 1

The effects of the materials bond parameter on impact, where (1) β is the bond strength, (2) $(r_x^{cm}, r_y^{cm}, r_z^{cm})$ is the final asteroid center of mass position, (3) $\frac{M_f}{M_o}$ is the ratio of final asteroid mass to original mass, (4) impact is the number of mass units hitting Earth (intersecting the Earth's surface) and (5) $\frac{M_I}{M_o}$ is the ratio asteroid mass impacting Earth to original asteroid mass (intersected with the Earth's surface).

β	r_x^{cm}	r_y^{cm}	r_z^{cm}	$\frac{M_f}{M_o}$	Impacts	$\frac{M_I}{M_o}$
1000	8.516	6.969	-9.422	1.0000	0	0.00
500	8.516	6.969	-9.422	1.0000	0	0.00
200	6.347	5.214	-9.530	0.9478	1	0.0002
100	3.677	3.010	-9.464	0.9228	1	0.0002
75	0.7853	3.3142	-5.636	0.9202	1555	0.3111
50	0.4634	0.3903	0.8046	0.9154	4745	0.9490

Table 2

The system parameters ($A_1 - A_{20}$) for the best performing gene with system weights of $w_1 = 1, w_2 = 0.01$. The pulse magnitudes are shown ($A_1 - A_5$) and the direction parameters (not normalized $A_6 - A_{20}$).

A_1	A_2	A_3	A_4	A_5	A_6	A_7	A_8	A_9	A_{10}	
371.9921	347.8975	173.8220	44.1396	87.1473	-0.1014	-0.01946	0.0069	-0.9742	-0.4718	
A_{11}	A_{12}	A_{13}	A_{14}	A_{15}	A_{16}	A_{17}	A_{18}	A_{19}	A_{20}	Π
0.4888	-0.6691	0.3889	0.5560	-0.5461	-0.1070	0.1927	-0.9651	-0.6106	-0.5510	0.089924

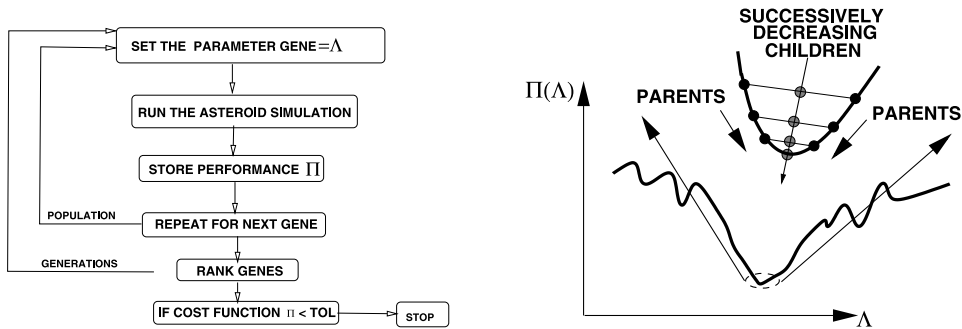


Fig. 9. A flowchart for the overall genetic-based machine-learning algorithm and its basic action (Zohdi [43–47]).

where the error in minimizing the mass of impacting asteroid material (normalized)

$$\Pi^{(1)} = \frac{M_I}{M_o} \tag{7.2}$$

and maximizing the distance between the center of Earth and the center of mass of the asteroid (normalized by the Earth's radius)

$$\Pi^{(2)} = \frac{R^{Earth}}{\|r^{Earth} - r^{cm,asteroid}\|} \tag{7.3}$$

We systematically minimize Eq. (7.1), $\min_{\Lambda} \Pi$, by varying the system parameters: $A^i \stackrel{\text{def}}{=} \{A_1^i, A_2^i, A_3^i, \dots, A_N^i\}$. The system parameter search is conducted within the constrained ranges of $A_1^{(-)} \leq A_1 \leq A_1^{(+)}$, $A_2^{(-)} \leq A_2 \leq A_2^{(+)}$, $A_3^{(-)} \leq A_3 \leq A_3^{(+)}$, etc. These upper and lower limits are dictated by what is physically feasible.

7.1. A genetic-based machine-learning algorithm (MLA)

Cost functions such as Π are nonconvex in system parameter space and often nonsmooth. Their minimization is usually difficult with direct application of gradient methods. This motivates nondervative search methods, for

example those found in machine-learning algorithms (MLA). One of the most basic subsets of MLA are so-called Genetic Algorithms (GA). For a review of GA, see the pioneering work of John Holland [48,49], as well as Goldberg [50], Davis [51], Onwubiko [52] and Goldberg and Deb [53]. A description of the algorithm will be described next (Zohdi [43–47]).

7.2. Algorithmic structure

The genetic-based MLA approach is extremely well-suited for nonconvex, nonsmooth, multicomponent, multi-stage systems and, broadly speaking, involves the following essential concepts (Fig. 9):

1. **POPULATION GENERATION:** Generate a parameter population of genetic strings: Λ^i
2. **PERFORMANCE EVALUATION:** Compute performance of each genetic string: $\Pi(\Lambda^i)$
3. **RANK STRINGS:** Rank them $\Lambda^i, i = 1, \dots, S$ from best to worst
4. **MATING PROCESS:** Mate pairs/produce offspring
5. **GENE ELIMINATION:** Eliminate poorly performing genetic strings
6. **POPULATION REGENERATION:** Repeat process with updated gene pool and new *random* genetic strings
7. **SOLUTION POST-PROCESSING:** Employ gradient-based methods afterwards in local *valleys-if smooth enough*

7.3. Specifics

Following Zohdi [43–47], the algorithm is as follows:

- **STEP 1:** Randomly generate a population of S starting genetic strings, $\Lambda^i, (i = 1, 2, 3, \dots, S)$:

$$\Lambda^i \stackrel{\text{def}}{=} \begin{Bmatrix} \Lambda_1^i \\ \Lambda_2^i \\ \Lambda_3^i \\ \dots \\ \Lambda_N^i \end{Bmatrix} \tag{7.4}$$

- **STEP 2:** Compute fitness of each string $\Pi(\Lambda^i), (i=1, \dots, S)$
- **STEP 3:** Rank genetic strings: $\Lambda^i, (i = 1, \dots, S)$ from best to worst
- **STEP 4:** Mate nearest pairs and produce two offspring, $(i = 1, \dots, S)$:

$$\lambda^i \stackrel{\text{def}}{=} \Phi \circ \Lambda^i + (\mathbf{1} - \Phi) \circ \Lambda^{i+1} \stackrel{\text{def}}{=} \begin{Bmatrix} \phi_1 \Lambda_1^i \\ \phi_2 \Lambda_2^i \\ \phi_3 \Lambda_3^i \\ \dots \\ \phi_N \Lambda_N^i \end{Bmatrix} + \begin{Bmatrix} (1 - \phi_1) \Lambda_1^{i+1} \\ (1 - \phi_2) \Lambda_2^{i+1} \\ (1 - \phi_3) \Lambda_3^{i+1} \\ \dots \\ (1 - \phi_N) \Lambda_N^{i+1} \end{Bmatrix} \tag{7.5}$$

and

$$\lambda^{i+1} \stackrel{\text{def}}{=} \Psi \circ \Lambda^i + (\mathbf{1} - \Psi) \circ \Lambda^{i+1} \stackrel{\text{def}}{=} \begin{Bmatrix} \psi_1 \Lambda_1^i \\ \psi_2 \Lambda_2^i \\ \psi_3 \Lambda_3^i \\ \dots \\ \psi_N \Lambda_N^i \end{Bmatrix} + \begin{Bmatrix} (1 - \psi_1) \Lambda_1^{i+1} \\ (1 - \psi_2) \Lambda_2^{i+1} \\ (1 - \psi_3) \Lambda_3^{i+1} \\ \dots \\ (1 - \psi_N) \Lambda_N^{i+1} \end{Bmatrix} \tag{7.6}$$

where for this operation, the ϕ_i and ψ_i are random numbers, such that $0 \leq \phi_i \leq 1, 0 \leq \psi_i \leq 1$, which are different for each component of each genetic string

- **STEP 5:** Eliminate the bottom M strings and keep top K parents and their K offspring (K offspring + K parents + $M = S$)
- **STEP 6:** Repeat STEPS 1–5 with top gene pool (K offspring and K parents), plus M new, randomly generated, strings
- **OPTIONS:**
- One can rescale and restart search around best performing parameter set every few generations, thus refocussing the computation effort around the most promising (optimal) areas of system parameter space.
- One can further apply a gradient-based method as a type of post-processing of the located global optimum, provided that the objective function in sufficiently smooth regions of the parameter space (see Luenberger [54] and Gill, Murray and Wright [55]).
- One can easily employ parallel processing for evaluating different genetic strings.

Remark. If one selects the mating parameters ϕ 's and ψ 's to be greater than one and/or less than zero, one can induce *mutations*, i.e. characteristics that neither parent possesses. However, this is somewhat redundant with introduction of new random members of the population in the current algorithm. If one does not retain the parents in the algorithm above, it is possible that inferior performing offspring may replace superior parents. Thus, top parents should be kept for the next generation. Additionally, retained parents do not need to be reevaluated in the next generation, making the algorithm less computationally expensive. Numerous studies of the author (Zohdi [43–47]) have shown that the advantages of parent retention outweighs inbreeding, for sufficiently large population sizes.

7.4. Algorithmic settings

In the upcoming example, the system parameters $\mathbf{A} = \{A_1, A_2, \dots, A_N\}$ are optimized over the search intervals (20 variables): $A_i^- \leq A_i \leq A_i^+$, $i = 1, 2, \dots, 20$. Specifically (Fig. 10), we varied the 20 parameters associated with pulse magnitudes and directions and used the following MLA settings⁸:

- Number of system variables: 20,
- Population size per generation: 24,
- Number of parents to keep in each generation: 6,
- Number of children created in each generation: 6,
- Number of completely new genes created in each generation: 12,
- Number of generations for re-adaptation around a new search interval: 10 and
- Number of generations: 50.

7.5. Parameter search ranges and results

We considered a 20 parameter system comprised of 5 thermonuclear pulses, consisting of 4 variables: one magnitude $\|\mathbf{F}\|$ and three direction components (d_1, d_2, d_3). The following search parameter ranges were used (with $w_1 = 1$ and $w_2 = 0.01$):

- Pulse Magnitudes: $A_{i=1-5} : A_i^- = 0 \leq A_i \leq A_i^+ = 400$,
- Pulse Directions: $A_{i=6-20} : A_i^- = -1 \leq A_i \leq A_i^+ = 1$.

Fig. 10 illustrates the results for the cost function for the best performing gene (*red*) as a function of successive generations, as well as the average performance cost function of the entire population of genes (*green*). We allowed the MLA/GA to readapt every 10 generations. Often, this action is more efficient than allowing the algorithm not to readapt, since it probes around the current optimum for better local alternatives, although for this model problem the effect was mild. The weights were set to $w_1 = 1$ and $w_2 = 0.01$. The final “subcost” functions were $w_1 \Pi^{(1)} = 0.088800$ and $w_2 \Pi^{(2)} = 0.001124$. The total cost was $\Pi^{total} = 0.089924$. The entire 50 generation simulation,

⁸ As in the previous example a standard Macbook Pro laptop was used for all calculations using a code written by the author. The same system parameters were used, and the fragmentation threshold value for dislodging of a particle was set to 75 N.

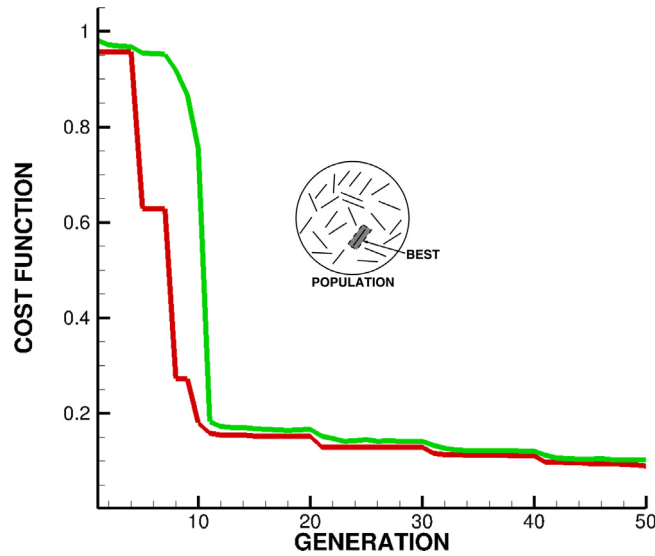


Fig. 10. Shown are the cost function for the best performing gene (*red*) as a function of successive generations, as well as the average cost function of the entire population of genes (*green*). We allowed the MLA/GA to readapt every 10 generations. Often, this action is more efficient than allowing the algorithm not to readapt, since it probes around the current optimum for better local alternatives. The weights were set to $w_1 = 1$ and $w_2 = 0.01$. The final “subcost” functions were $w_1\Pi^{(1)} = 0.088800$ and $w_2\Pi^{(2)} = 0.001124$. The total cost was $\Pi^{total} = 0.089924$. (For interpretation of the references to color in this figure legend, the reader is referred to the web version of this article.)

with 24 genes per evaluation (480 total parameter sets) took a few minutes on a laptop, *making it ideal as an evaluation tool*. We note that, for a given set of parameters, a complete simulation takes approximately one second, thus hundreds of parameter sets can be evaluated in an hour, *without even exploiting the inherent parallelism of the genetic-based MLA*. The speed at which the overall process can be completed makes it a suitable digital-twin of the system that can run in real-time or faster than the actual physical system, making it suitable as either an evaluation tool or an adaptive controller. Considering the serious nature of the problems considered, adaptive control of such devices is paramount.

8. Summary and extensions

As indicated at the outset of this work, detection capabilities in astronomy have dramatically improved and the development of strategies to mitigate a collision between Earth and large *Planet Killer Asteroids* (PKAs) are under development. Harnessing the enormous energy of nuclear devices has been proposed for a number of years to destroy or deflect asteroids that are on a projected collision course with Earth. Two main mitigation strategies have been proposed:

- **Case 1:** Break up an incoming asteroid into smaller pieces that will disperse widely, resulting in smaller-scale, less detrimental, Earth-impacts or
- **Case 2:** Deflect an incoming asteroid trajectory to avoid collision altogether.

This work developed a computational framework to rapidly simulate the dynamical response of a PKA to a series of ultra-high energy impulses, such as those generated by nuclear devices, using a Discrete Element Method (DEM) method. This allows for rapid determination of the fragmentation of the PKA and the trajectories and distribution of the resulting debris field. When coupled to a machine-learning algorithm, this allows one to optimize the pulsation strategy for maximum possible safety and success. The following topics represent areas for extending this work:

- **PKA-fragment interaction:** Once a DEM cluster of bonded particles breaks up, the calculation of the interaction between the fragments, involving a full contact analysis, is a logical extension of the analysis

presented in this work. A relatively straightforward direct numerical simulation (DNS) formulation of the dynamics of a multi-particulate system is to track the motion of $i = 1, 2, \dots, N$ particles, and to solve

$$m_i \ddot{\mathbf{r}}_i = \mathbf{F}_i^{tot}(\mathbf{r}_1, \mathbf{r}_2, \dots, \mathbf{r}_N) + \text{constraints}, \quad (8.1)$$

where \mathbf{r}_i is the position vector of the i th particle, \mathbf{F}_i^{tot} represents all forces acting on particle i . In such cases, the entire coupled system can be efficiently solved recursively within each time step, thus producing a fixed point iteration of the form:

$$\mathbf{r}_i^{K+1}(t + \Delta t) = \mathcal{F}(\mathbf{r}_i^K(t + \Delta t)) + \mathbf{R}. \quad (8.2)$$

The convergence of such a scheme scales with the time-step size, which necessitate adaptive time-stepping schemes (see [Appendix B](#)). The simulation of such flowing particulate systems, in addition to the corresponding multibody contact mechanics, has been extensively investigated for the last decade by Zohdi [37–42], employing numerical schemes based on high-performance iterative solvers, sorting–binning for fast inter-particle calculations, Verlet lists, domain decomposition and parallel processing. These types of formulations can efficiently compute the interaction of multiple fragments from breakup/disintegration, where the application of continuum approaches would be extremely difficult. The dynamics of fragments of clusters that evolve and interact with the asteroid and other fragments is complex, and is very closely related to the field of the mechanics of granular and particulate media, for example see Duran [56], Pöschel and Schwager [57], Onate et al. [58,59], Rojek et al. [60], Carbonell et al. [61] and Labra and Onate [62] and Zohdi [37–42].

- Detailed detonation stress and multiphysics analysis:** The use of high-precision continuum models for the stress analysis of such systems, while computationally expensive, is perhaps warranted to plan detonations more carefully. One key method that should be coupled to Discrete Element Methods for fragmentation are Voxel-based methods, which leverage image-based analyses, such as those found in Zohdi [63], whereby a voxel (3D *volume pixel*) representation of microstructures and corresponding digital solution methods are employed that avoid computationally expensive steps involved in usual Finite Element procedures, such as topologically conforming meshing, mapping, volume integration, stiffness matrix generation and matrix-based solution methods. The process proceeds by converting the material microstructure into voxels and the computations become *digital* on a regular *voxel-grid*, allowing extremely fast methods to be used to construct derivatives and to solve the system. These methods are ideal for heterogeneous irregular structures, consistent with digital, astronomical, pixel-based images. Finally, as mentioned earlier, while a nuclear weapon is a more powerful version of a conventional weapon, it has another component, it is *thermo-nuclear*, thus potentially leading to melting, fissuring, etc. which goes beyond simply a mechanical force blast, with approximately 50% being blast energy, 15% nuclear radiation and 35% thermal energy. Thus, more detailed models should involve multiphysical calculations of the thermal fields by solving the first law of thermodynamics, coupled to a balance of linear momentum. This will almost certainly necessitate the use of adaptive, implicit, staggering schemes ([Appendix B](#)) to solve the coupled system. We refer readers to Zohdi [37–42] for studies of this type. These extensions are under current investigation by the author.

Declaration of competing interest

The author declare that he has no known competing financial interests or personal relationships that could have appeared to influence the work reported in this paper.

Data availability

No data was used for the research described in the article.

Acknowledgments

This work was funded in part by the Department of Energy, Sandia National Labs and the College of Engineering at UC Berkeley, USA.

Appendix A. Temporal discretization

Consider a generic particle's equation of motion, given by

$$m\dot{\mathbf{v}} = \mathbf{F}, \quad (\text{A.1})$$

where \mathbf{F} is the force provided from interactions with other particles and the external environment. Expanding the velocity in a Taylor series about $t + \phi\Delta t$ we obtain ($0 \leq \phi \leq 1$)

$$\mathbf{v}(t + \Delta t) = \mathbf{v}(t + \phi\Delta t) + \frac{d\mathbf{v}}{dt}\Big|_{t+\phi\Delta t}(1 - \phi)\Delta t + \frac{1}{2}\frac{d^2\mathbf{v}}{dt^2}\Big|_{t+\phi\Delta t}(1 - \phi)^2(\Delta t)^2 + \mathcal{O}(\Delta t)^3 \quad (\text{A.2})$$

and

$$\mathbf{v}(t) = \mathbf{v}(t + \phi\Delta t) - \frac{d\mathbf{v}}{dt}\Big|_{t+\phi\Delta t}\phi\Delta t + \frac{1}{2}\frac{d^2\mathbf{v}}{dt^2}\Big|_{t+\phi\Delta t}\phi^2(\Delta t)^2 + \mathcal{O}(\Delta t)^3. \quad (\text{A.3})$$

Subtracting the two expressions yields

$$\frac{d\mathbf{v}}{dt}\Big|_{t+\phi\Delta t} = \frac{\mathbf{v}(t + \Delta t) - \mathbf{v}(t)}{\Delta t} + \hat{\mathcal{O}}(\Delta t), \quad (\text{A.4})$$

where $\hat{\mathcal{O}}(\Delta t) = \mathcal{O}(\Delta t)^2$ when $\phi = \frac{1}{2}$. Inserting this into the equation of motion yields

$$\mathbf{v}(t + \Delta t) = \mathbf{v}(t) + \frac{\Delta t}{m}\mathbf{F}(t + \phi\Delta t) + \hat{\mathcal{O}}(\Delta t)^2. \quad (\text{A.5})$$

Note that adding a weighted sum of Eqs. (A.2) and (A.3) yields

$$\mathbf{v}(t + \phi\Delta t) = \phi\mathbf{v}(t + \Delta t) + (1 - \phi)\mathbf{v}(t) + \mathcal{O}(\Delta t)^2, \quad (\text{A.6})$$

which will be useful shortly. Now expanding the position of the center of mass in a Taylor series about $t + \phi\Delta t$ we obtain

$$\mathbf{r}(t + \Delta t) = \mathbf{r}(t + \phi\Delta t) + \frac{d\mathbf{r}}{dt}\Big|_{t+\phi\Delta t}(1 - \phi)\Delta t + \frac{1}{2}\frac{d^2\mathbf{r}}{dt^2}\Big|_{t+\phi\Delta t}(1 - \phi)^2(\Delta t)^2 + \mathcal{O}(\Delta t)^3 \quad (\text{A.7})$$

and

$$\mathbf{r}(t) = \mathbf{r}(t + \phi\Delta t) - \frac{d\mathbf{r}}{dt}\Big|_{t+\phi\Delta t}\phi\Delta t + \frac{1}{2}\frac{d^2\mathbf{r}}{dt^2}\Big|_{t+\phi\Delta t}\phi^2(\Delta t)^2 + \mathcal{O}(\Delta t)^3. \quad (\text{A.8})$$

Subtracting the two expressions yields

$$\frac{\mathbf{r}(t + \Delta t) - \mathbf{r}(t)}{\Delta t} = \mathbf{v}(t + \phi\Delta t) + \hat{\mathcal{O}}(\Delta t). \quad (\text{A.9})$$

Inserting Eq. (A.6) yields

$$\mathbf{r}(t + \Delta t) = \mathbf{r}(t) + (\phi\mathbf{v}(t + \Delta t) + (1 - \phi)\mathbf{v}(t))\Delta t + \hat{\mathcal{O}}(\Delta t)^2 \quad (\text{A.10})$$

and thus using Eq. (A.5) yields

$$\mathbf{r}(t + \Delta t) = \mathbf{r}(t) + \mathbf{v}(t)\Delta t + \frac{\phi(\Delta t)^2}{m}\mathbf{F}(t + \phi\Delta t) + \hat{\mathcal{O}}(\Delta t)^2. \quad (\text{A.11})$$

The term $\mathbf{F}(t + \phi\Delta t)$ can be approximated by

$$\mathbf{F}(t + \phi\Delta t) \approx \phi\mathbf{F}(\mathbf{r}(t + \Delta t)) + (1 - \phi)\mathbf{F}(\mathbf{r}(t)), \quad (\text{A.12})$$

yielding

$$\mathbf{r}(t + \Delta t) = \mathbf{r}(t) + \mathbf{v}(t)\Delta t + \frac{\phi(\Delta t)^2}{m}(\phi\mathbf{F}(\mathbf{r}(t + \Delta t)) + (1 - \phi)\mathbf{F}(\mathbf{r}(t))) + \hat{\mathcal{O}}(\Delta t)^2. \quad (\text{A.13})$$

We note that

- When $\phi = 1$, then this is the (implicit) Backward Euler scheme, which is very stable (very dissipative) and $\mathcal{O}(\Delta t)^2$ locally in time,

- When $\phi = 0$, then this is the (explicit) Forward Euler scheme, which is conditionally stable and $\mathcal{O}(\Delta t)^2$ locally in time,
- When $\phi = 0.5$, then this is the (implicit) ‘‘Midpoint’’ scheme, which is stable and $\hat{\mathcal{O}}(\Delta t)^2 = \mathcal{O}(\Delta t)^3$ locally in time.

Appendix B. Temporally adaptive iterative schemes

For illustration purposes, after time discretization of the acceleration term in the equations of motion $m\ddot{\mathbf{r}} = \Psi$ using a ϕ -method

$$\mathbf{r}^{L+1} = \mathbf{r}^L + \mathbf{v}^L \Delta t + \frac{\phi(\Delta t)^2}{m} (\phi \mathbf{F}(\mathbf{r}^{L+1}) + (1 - \phi) \mathbf{F}(\mathbf{r}^L)), \tag{B.1}$$

one arrives at the following abstract form, for the entire system of particles,

$$\mathcal{A}(\mathbf{r}^{L+1}) = \mathcal{F}. \tag{B.2}$$

It is convenient to write

$$\mathcal{A}(\mathbf{r}^{L+1}) - \mathcal{F} = \mathcal{G}(\mathbf{r}^{L+1}) - \mathbf{r}^{L+1} + \mathcal{R} = \mathbf{0}, \tag{B.3}$$

where \mathcal{R} is a remainder term that does not depend on the solution, i.e. $\mathcal{R} \neq \mathcal{R}(\mathbf{r}^{L+1})$. A straightforward iterative scheme can be written as

$$\mathbf{r}^{L+1,K} = \mathcal{G}(\mathbf{r}^{L+1,K-1}) + \mathcal{R}, \tag{B.4}$$

where $K = 1, 2, 3, \dots$ is the index of iteration within time step $L + 1$. The convergence of such a scheme is dependent on the behavior of \mathcal{G} . Namely, a sufficient condition for convergence is that \mathcal{G} is a contraction mapping for all $\mathbf{r}^{L+1,K}$, $K = 1, 2, 3, \dots$. In order to investigate this further, we define the iteration error as $\varepsilon^{L+1,K} \stackrel{\text{def}}{=} \mathbf{r}^{L+1,K} - \mathbf{r}^{L+1}$. A necessary restriction for convergence is iterative self consistency, i.e. the ‘‘exact’’ (discretized) solution must be represented by the scheme

$$\mathcal{G}(\mathbf{r}^{L+1}) + \mathcal{R} = \mathbf{r}^{L+1}. \tag{B.5}$$

Enforcing this restriction, a sufficient condition for convergence is the existence of a contraction mapping

$$\varepsilon^{L+1,K} = \|\mathbf{r}^{L+1,K} - \mathbf{r}^{L+1}\| = \|\mathcal{G}(\mathbf{r}^{L+1,K-1}) - \mathcal{G}(\mathbf{r}^{L+1})\| \tag{B.6}$$

$$\leq \eta^{L+1,K} \|\mathbf{r}^{L+1,K-1} - \mathbf{r}^{L+1}\|, \tag{B.7}$$

where, if $0 \leq \eta^{L+1,K} < 1$ for each iteration K , then $\varepsilon^{L+1,K} \rightarrow \mathbf{0}$ for any arbitrary starting value $\mathbf{r}^{L+1,K=0}$, as $K \rightarrow \infty$. This type of contraction condition is sufficient, but not necessary, for convergence. Inserting this into $m\ddot{\mathbf{r}} = \Psi(\mathbf{r})$ leads to

$$\mathbf{r}^{L+1,K} = \underbrace{\mathbf{r}^L + \mathbf{v}^L \Delta t + \frac{\phi(\Delta t)^2}{m} ((1 - \phi) \mathbf{F}(\mathbf{r}^L))}_{\mathcal{R}} + \underbrace{\frac{\phi(\Delta t)^2}{m} (\phi \mathbf{F}(\mathbf{r}^{L+1,K-1}))}_{\mathcal{G}(\mathbf{r}^{L+1,K-1})}, \tag{B.8}$$

whose convergence is restricted by $\eta \propto \frac{(\phi \Delta t)^2}{m}$. Therefore, we see that the contraction constant of \mathcal{G} is (1) directly dependent on the strength of the interaction forces, (2) inversely proportional to m and (3) directly proportional to $\phi \Delta t$. Therefore, if convergence is slow within a time step, the time step size, which is adjustable, can be reduced by an appropriate amount to increase the rate of convergence. Thus, decreasing the time step size improves the convergence, however, we want to simultaneously maximize the time-step sizes to decrease overall computing time, while still meeting an error tolerance on the numerical solution’s accuracy. In order to achieve this goal, we follow an approach found in Zohdi [37–42] originally developed for continuum thermo-chemical multifield problems in which (1) one approximates

$$\eta^{L+1,K} \approx S(\Delta t)^p \tag{B.9}$$

(S is a constant) and (2) one assumes that the error within an iteration to behave according to

$$(S(\Delta t)^p)^K \varepsilon^{L+1,0} = \varepsilon^{L+1,K}, \tag{B.10}$$

$K = 1, 2, \dots$, where $\varepsilon^{L+1,0}$ is the initial norm of the iterative error and S is intrinsic to the system.⁹ Our goal is to meet an error tolerance in exactly a preset number of iterations. To this end, one writes

$$(S(\Delta t_{\text{tol}})^p)^{K_d} \varepsilon^{L+1,0} = TOL, \tag{B.11}$$

where TOL is a tolerance and where K_d is the number of desired iterations.¹⁰ If the error tolerance is not met in the desired number of iterations, the contraction constant $\eta^{L+1,K}$ is too large. Accordingly, one can solve for a new smaller step size, under the assumption that S is constant,

$$\Delta t_{\text{tol}} = \Delta t \left(\frac{(\frac{TOL}{\varepsilon^{L+1,0}})^{\frac{1}{pK_d}}}{(\frac{\varepsilon^{L+1,K}}{\varepsilon^{L+1,0}})^{\frac{1}{pK}}} \right). \tag{B.12}$$

The assumption that S is constant is not critical, since the time steps are to be recursively refined and unrefined throughout the simulation. Clearly, the expression in Eq. (B.12) can also be used for time step enlargement, if convergence is met in less than K_d iterations.¹¹ An implementation of the procedure is as follows for a multiparticle system:

(1) GLOBAL FIXED – POINT ITERATION (SET $i = 1$ AND $K = 0$) :

(2) IF $i > N_p$ THEN GO TO (4)

(3) IF $i \leq N_p$ THEN :

(a) COMPUTE POSITION : $r_i^{L+1,K}$

(b) GO TO (2) FOR NEXT PARTICLE ($i = i + 1$)

(4) ERROR MEASURE :

(a) $\varepsilon_K \stackrel{\text{def}}{=} \frac{\sum_{i=1}^{N_p} \|r_i^{L+1,K} - r_i^{L+1,K-1}\|}{\sum_{i=1}^{N_p} \|r_i^{L+1,K} - r_i^L\|}$ (normalized)

(b) $Z_K \stackrel{\text{def}}{=} \frac{\varepsilon_K}{TOL_r}$

(c) $\Phi_K \stackrel{\text{def}}{=} \left(\frac{(\frac{TOL}{\varepsilon_0})^{\frac{1}{pK_d}}}{(\frac{\varepsilon_K}{\varepsilon_0})^{\frac{1}{pK}}} \right)$

(5) IF TOLERANCE MET ($Z_K \leq 1$) AND $K < K_d$ THEN :

(a) INCREMENT TIME : $t = t + \Delta t$

(b) CONSTRUCT NEW TIME STEP : $\Delta t = \Phi_K \Delta t$,

(c) SELECT MINIMUM : $\Delta t = \text{MIN}(\Delta t^{lim}, \Delta t)$ AND GO TO (1)

(6) IF TOLERANCE NOT MET ($Z_K > 1$) AND $K = K_d$ THEN :

(a) CONSTRUCT NEW TIME STEP : $\Delta t = \Phi_K \Delta t$

(b) RESTART AT TIME = t AND GO TO (1)

Generally speaking, the iterative error, which is a function of the time step size, is temporally variable and can become stronger, weaker, or possibly oscillatory, is extremely difficult to ascertain a-priori as a function of the time step size. Therefore, to circumvent this problem, the adaptive strategy presented in this section was developed to provide accurate solutions by iteratively adjusting the time steps. Specifically, a sufficient condition for the convergence of the presented fixed-point scheme was that the spectral radius or contraction constant of the coupled operator, which depends on the time step size, must be less than unity. This observation was used to adaptively maximize the time step sizes, while simultaneously controlling the coupled operator’s spectral radius, in order to deliver solutions below an error tolerance within a prespecified number of desired iterations. This recursive staggering error control can allow for substantial reduction of computational effort by the adaptive use of large time steps. Furthermore, such a recursive process has a reduced sensitivity, relative to an explicit staggering approach, to the order in which the individual equations are solved, since it is self-correcting.

⁹ For the class of problems under consideration, due to the quadratic dependency on Δt , $p \approx 2$.

¹⁰ Typically, K_d is chosen to be between five to ten iterations.

¹¹ Time-step size adaptivity is important, since the system’s dynamics can dramatically change over the course of time, possibly requiring quite different time step sizes to control the iterative error. However, to maintain the accuracy of the time-stepping scheme, one must respect an upper bound dictated by the discretization error, i.e., $\Delta t \leq \Delta t^{lim}$.

Remark. With regard to the solution process, a recursive iterative scheme of the Jacobi-type, where the updates are made only after one complete system iteration, was illustrated in the derivations only for algebraic simplicity. The Jacobi method is easier to address theoretically, while the Gauss–Seidel type method, which involves immediately using the most current values, when they become available, is usually used at the implementation level. As is well-known, under relatively general conditions, if the Jacobi method converges, the Gauss–Seidel method converges at a faster rate, while if the Jacobi method diverges, the Gauss–Seidel method diverges at a faster rate (for example, see Ames [64] or Axelsson [65]). It is important to realize that the Jacobi method is perfectly parallelizable. In other words, the calculation for each particle are uncoupled, with the updates only coming afterwards. Gauss–Seidel, since it requires the most current updates, couples the particle calculations immediately. However, these methods can be combined to create hybrid approaches, whereby the entire particulate flow is partitioned into groups and within each group a Gauss–Seidel method is applied. In other words, for a group, the positions of any particles from outside are initially frozen, as far as calculations involving members of the group are concerned. After each isolated group’s solution (particle positions) has converged, computed in parallel, then all positions are updated, i.e. the most current positions become available to all of the particles in the system, and the isolated group calculations are repeated. Classical solution methods require $\mathcal{O}(N^3)$ operations, whereas iterative schemes, such as the one presented, typically require order N^q , where $1 \leq q \leq 2$. For details see Axelsson [65]. Also, such solvers are highly advantageous since solutions to previous time steps can be used as the first guess to accelerate the solution procedure.

References

- [1] L.W. Alvarez, W. Alvarez, F. Asaro, H.V. Michel, Extraterrestrial cause for the cretaceous-tertiary extinction: Experiment and theory (PDF), *Science* 208 (4448) (1980) 1095–1108, <http://dx.doi.org/10.1126/science.208.4448.1095>, Bibcode:1980Sci...208.1095A. JSTOR 1683699. PMID 17783054. S2CID 16017767.
- [2] NASA double asteroid redirection test, 2021, <https://www.nasa.gov/planetarydefense/dart/dart-news> <https://solarsystem.nasa.gov/resources/2668/nasas-first-asteroid-deflection-test/>.
- [3] NASA is practicing asteroid deflection. You know, just in case. <https://www.theatlantic.com/science/archive/2021/11/nasa-asteroid-mission-planetary-defense/620822/> The Atlantic.
- [4] D. Izzo, A. Bourdoux, R. Walker, F. Ongaro, Optimal Trajectories for the Impulsive Deflection of NEOs; Paper IAC-05-C1.5.06, 56th International Astronautical Congress, Fukuoka, Japan, (October 2005), Vol. 59, 2006, pp. 294–300, Later published in *Acta Astronautica*, No. 1-5.
- [5] A. Carusi, G. D’Abramo, G. Valsecchi, Orbital and mission planning constraints for the deflection of NEOs impacting on earth, *Icarus* 194 (2) (2008) 450–462.
- [6] Russell L. Schweickart, Edward T. Lu, Piet Hut, Clark R. Chapman, The asteroid tugboat, *Sci. Am.* 289 (5) (2003) 54–61, JSTOR 26060526.
- [7] M.J.S. Belton, *Mitigation of Hazardous Comets and Asteroids*, Cambridge University Press, ISBN: 0521827647, 2004, 978-0521827645.
- [8] John S. Lewis, *Comet and Asteroid Impact Hazards on a Populated Earth: Computer Modeling (Volume 1 of Comet and Asteroid Impact Hazards on a Populated Earth: Computer Modeling)*, Academic Press, ISBN: 0124467601, 2000, 978-0124467606.
- [9] Gerrit L. Verschuur, *Impact!: The Threat of Comets and Asteroids*, Oxford University Press, ISBN: 0195353277, 1997, 978-0195353273.
- [10] Charles El Mir, K.T. Ramesh, Derek C. Richardson, A new hybrid framework for simulating hypervelocity asteroid impacts and gravitational reaccumulation, *Icarus* 321 (2019) 1013–1025, <http://dx.doi.org/10.1016/j.icarus.2018.12.032>, Bibcode:2019Icar.321.1013E. S2CID 127119234.
- [11] Paul Chodas, Shakeh Khudikyan, Alan Chamberlin, *Planetary Defense Conference Exercise - 2021 Planetary Defense Conference (Virtually) in Vienna, Austria, April 26-April 30, 2021*, NASA, 2021, Retrieved 14 May 2021.
- [12] G.H. Canavan, J.C. Solem, Interception of near-Earth objects, *Mercury* (ISSN: 0047-6773) 21 (3) (1992) 107–109, Bibcode:1992Merqu...21..107C.
- [13] C.D. Hall, I.M. Ross, Dynamics and control problems in the deflection of near-earth objects, in: *Advances in the Astronautical Sciences, Astrodynamics 1997*, Vol. 97, Part I, 1997, pp. 613–631.
- [14] J.C. Solem, Interception of comets and asteroids on collision course with earth, *J. Spacecr. Rockets* 30 (2) (1993) 222–228, <http://dx.doi.org/10.2514/3.11531>, Bibcode:1993JSpRo.30.222S.
- [15] J.C. Solem, Deflection and disruption of asteroids on collision course with Earth, *J. Br. Interplanet. Soc.* 53 (2000) 180–196, Bibcode:2000JBIS.53.180S.
- [16] E. Asphaug, S.J. Ostro, R.S. Hudson, D.J. Scheeres, W. Benz, Disruption of kilometre-sized asteroids by energetic collisions(PDF), *Nature* 393 (6684) (1998) 437–440, <http://dx.doi.org/10.1038/30911>, Bibcode:1998Natur.393..437A. S2CID 4328861. Archived from the original (PDF) on March 6, 2016.
- [17] H.J. Melosh, I.V. Nemchinov, Solar asteroid diversion, *Nature* (ISSN: 0028-0836) 366 (6450) (1993) 21–22, <http://dx.doi.org/10.1038/366021a0>, Bibcode:1993Natur.366...21M. S2CID 4367291.
- [18] V.P. Vasylyev, Deflection of hazardous near-earth objects by high concentrated sunlight and adequate design of optical collector, *Earth Moon Planets* (ISSN: 0167-9295) 110 (1–2) (2012) 67–79, <http://dx.doi.org/10.1007/s11038-012-9410-2>, S2CID 120563921.

- [19] Zachary Fletcher, Kyle Ryan, Bryan Maas, Joseph Dickman, Randolph Hammond, Dmitriy Bekker, Tyler Nelson, James Mize, Jacob Greenberg, Wendy Hunt, Stephen Smece, Nancy Chabot, Andrew Cheng, Design of the didymos reconnaissance and asteroid camera for OpNav (DRACO) on the double asteroid redirection test (DART), in: Space Telescopes and Instrumentation 2018: Optical, Infrared, and Millimeter Wave. Vol. 106981X, Proceedings of SPIE, Austin, TX, 2018, p. 10698, <http://dx.doi.org/10.1117/12.2310136>.
- [20] Brian Kantsiper, The double asteroid redirection test (DART) mission electric propulsion trade, in: 2017 IEEE Aerospace Conference, ISBN: 978-1-5090-1613-6, 2017, pp. 1–7, <http://dx.doi.org/10.1109/AERO.2017.7943736>, S2CID 43072949.
- [21] Elena Adams, Daniel Oshaughnessy, Matthew Reinhart, Jeremy John, Elizabeth Congdon, Daniel Gallagher, Elisabeth Abel, Justin Atchison, Zachary Fletcher, Michelle Chen, Christopher Heistand, Philip Huang, Evan Smith, Deane Sibol, Dmitriy Bekker, David Carrelli, Double asteroid redirection test: The earth strikes back, in: 2019 IEEE Aerospace Conference, ISBN: 978-1-5386-6854-2, 2019, pp. 1–11, <http://dx.doi.org/10.1109/AERO.2019.8742007>, S2CID 195222414.
- [22] A.F. Cheng, P. Michel, C. Reed, A. Galvez, I. Carnelli, DART: Double asteroid redirection test (PDF), in: European Planetary Science Congress 2012. EPSC Abstracts, 2012.
- [23] P. Michel, A. Cheng, I. Carnelli, A. Rivkin, A. Galvez, S. Ulamec, C. Reed, AIDA Team, AIDA: Asteroid impact and deflection assessment mission under study at ESA and NASA, in: Spacecraft Reconnaissance of Asteroid and Comet Interiors, Vol. 1829, 2015, p. 6008, Bibcode:2015LPICo1829.6008M.
- [24] Andrew S. Rivkin, Nancy L. Chabot, Angela M. Stickle, Cristina A. Thomas, Derek C. Richardson, Olivier Barnouin, Eugene G. Fahnestock, Carolyn M. Ernst, Andrew F. Cheng, Steven Chesley, Shantanu Naidu, The double asteroid redirection test (DART): Planetary defense investigations and requirements, Planet. Sci. J. (ISSN: 2632-3338) 2 (5) (2021) 173, <http://dx.doi.org/10.3847/PSJ/ac063e>, Bibcode:2021PSJ.....2..173R. S2CID 237301576.
- [25] Patrick Michel, Michael Kueppers, Holger Sierks, Ian Carnelli, European component of the AIDA mission to a binary asteroid: Characterization and interpretation of the impact of the DART mission (PDF), Adv. Space Res. (Article) 62 (8) (2017) 2261–2272, <http://dx.doi.org/10.1016/j.asr.2017.12.020>, (published 18 December 2017).
- [26] Justin A. Atchison, Martin T. Ozimek, Brian L. Kantsiper, Andrew F. Cheng, Trajectory options for the DART mission, Acta Astronaut. (ISSN: 0094-5765) 123 (2016) 330–339, <http://dx.doi.org/10.1016/j.actaastro.2016.03.032>, Special Section: Selected Papers from the International Workshop on Satellite Constellations and Formation Flying 2015. Bibcode:2016AcAau.123.330A.
- [27] National Near-Earth Object Preparedness Strategy Action Plan (PDF), (Report), 2018, [whitehouse.gov](http://www.whitehouse.gov) Retrieved 22 2018- via National Archives.
- [28] Nathan Myhrvold, An empirical examination of WISE/NEOWISE asteroid analysis and results, Icarus 314 (2018) 64–97, <http://dx.doi.org/10.1016/j.icarus.2018.05.004>, Bibcode:2018Icar.314.64M.
- [29] Threats from Space: A Review of U.S. Government Efforts to Track and Mitigate Asteroids and Meteors (PDF) (Report). Hearing before the Committee on Science, Space, and Technology. Vol. Part I and Part II, House of Representatives, 2013, p. 147, Retrieved 26 November 2018.
- [30] Unusual Minor Planets. Minor Planet Center. International Astronomical Union. Retrieved 27 December 2018.
- [31] Cumulative Totals. Jet Propulsion Laboratory. Discovery Statistics, NASA, 2018, Retrieved 27 December 2018.
- [32] M. Beech, D. Steel, On the definition of the term meteoroid, Q. J. R. Astron. Soc. 36 (3) (1995) 281–284, Bibcode:1995QJRAS.36.281B. Meteoroid: A solid object moving in space, with a size less than 10 m, but larger than 100 μ m.
- [33] Atomic archive-the energy from a nuclear weapon. <https://www.atomicarchive.com/science/effects/energy.html>.
- [34] Wikipedia-nuclear weapon. https://en.wikipedia.org/wiki/Nuclear_weapon.
- [35] A. Tikkanen, Tsar bomba-soviet nuclear bomb, in: Encyclopedia Britannica, 2022, <https://www.britannica.com/topic/Tsar-Bomba>.
- [36] D. Powell, T.I. Zohdi, Attachment mode performance of network-modeled ballistic fabric shielding, Composites B 40 (6) (2009) 451–460.
- [37] T.I. Zohdi, An adaptive-recursive staggering strategy for simulating multifield coupled processes in microheterogeneous solids, Internat. J. Numer. Methods Engrg. 53 (2002) 1511–1532.
- [38] T.I. Zohdi, Modeling and simulation of a class of coupled thermo-chemo-mechanical processes in multiphase solids, Comput. Methods Appl. Mech. Eng. 193 (6-8) (2004) 679–699.
- [39] T.I. Zohdi, A computational framework for agglomeration in thermo-chemically reacting granular flows, Proc. R. Soc. 460 (2052) (2004) 3421–3445.
- [40] T.I. Zohdi, P-wave induced energy and damage distribution in agglomerated granules, Modelling Simulation Mater. Sci. Eng. 15 (2007) S435–S448.
- [41] T.I. Zohdi, Numerical simulation of charged particulate cluster-droplet impact on electrified surfaces, J. Comput. Phys. 233 (2013) 509–526.
- [42] T.I. Zohdi, On progressive blast envelope evolution of charged particles in electromagnetic fields, Comput. Methods Appl. Mech. Engrg. (2016) <http://dx.doi.org/10.1016/j.cma.2016.05.003>.
- [43] T.I. Zohdi, Dynamic thermomechanical modeling and simulation of the design of rapid free-form 3D printing processes with evolutionary machine learning, Comput. Methods Appl. Mech. Engrg. 331 (2018) 343–362.
- [44] T.I. Zohdi, Electrodynamic machine-learning-enhanced fault-tolerance of robotic free-form printing of complex mixtures, Comput. Mech. 63 (2019) 913–929.
- [45] T.I. Zohdi, A machine-learning framework for rapid adaptive digital-twin based fire-propagation simulation in complex environments, Comput. Methods Appl. Mech. Engrg. 363 (2020) 112907.
- [46] T.I. Zohdi, A digital twin framework for machine learning optimization of aerial fire fighting and pilot safety, Comput. Methods Appl. Mech. Engrg. 373 (2021) 113446, 1 January 2021.
- [47] T.I. Zohdi, A digital-twin and machine-learning framework for the design of multiobjective agrophotovoltaic solar farms, Comput. Mech. (2021) <http://dx.doi.org/10.1007/s00466-021-02035-z>.

- [48] J.H. Holland, *Adaptation in Natural & Artificial Systems*, University of Michigan Press, Ann Arbor, Mich, 1975.
- [49] J.H. Holland, J.H. Miller, Artificial adaptive agents in economic theory (PDF), *Amer. Econ. Rev.* 81 (2) (1991) 365–371, Archived from the original (PDF) on October 27, 2005.
- [50] D.E. Goldberg, *Genetic Algorithms in Search, Optimization & Machine Learning*, Addison-Wesley, 1989.
- [51] L. Davis, *Handbook of Genetic Algorithms*, Thompson Computer Press, 1991.
- [52] C. Onwubiko, *Introduction to Engineering Design Optimization*, Prentice Hall, 2000.
- [53] D.E. Goldberg, K. Deb, Special issue on genetic algorithms, *Comput. Methods Appl. Mech. Engrg.* 186 (2–4) (2000) 121–124.
- [54] D. Luenberger, *Introduction to Linear & Nonlinear Programming*, Addison-Wesley, Menlo Park, 1974.
- [55] P. Gill, W. Murray, M. Wright, *Practical Optimization*, Academic Press, 1995.
- [56] J. Duran, Sands, *Powders and Grains. An Introduction to the Physics of Granular Matter*, Springer Verlag, 1997.
- [57] T. Pöschel, T. Schwager, *Computational Granular Dynamics*, Springer Verlag, 2004.
- [58] E. Onate, S.R. Idelsohn, M.A. Celigueta, R. Rossi, Advances in the particle finite element method for the analysis of fluid-multibody interaction and bed erosion in free surface flows, *Comput. Methods Appl. Mech. Engrg.* 197 (19–20) (2008) 1777–1800.
- [59] E. Onate, M.A. Celigueta, S.R. Idelsohn, F. Salazar, B. Suárez, Possibilities of the particle finite element method for fluid-soil–structure interaction problems, *Comput. Mech.* 48 (2011) 307–318.
- [60] J. Rojek, C. Labra, O. Su, E. Onate, Comparative study of different discrete element models and evaluation of equivalent micromechanical parameters, *Int. J. Solids Struct.* 49 (2012) 1497–1517, <http://dx.doi.org/10.1016/j.ijsolstr.2012.02.032>.
- [61] J.M. Carbonell, E. Onate, B. Suarez, Modeling of ground excavation with the particle finite element method, *ASCE J. Eng. Mech.* 136 (2010) 455–463.
- [62] C. Labra, E. Onate, High-density sphere packing for discrete element method simulations, *Commun. Numer. Methods. Eng.* 25 (7) (2009) 837–849.
- [63] T.I. Zohdi, Rapid voxel-based digital-computation for complex microstructured media, *Arch. Comput. Methods Eng.* (2018) <http://dx.doi.org/10.1007/s11831-018-9284-1>.
- [64] W.F. Ames, *Numerical Methods for Partial Differential Equations*, second ed., Academic Press, 1977.
- [65] O. Axelsson, *Iterative Solution Methods*, Cambridge University Press, 1994.